

# Numerical and Experimental Investigation of Performance and Flooding Phenomena of a PEM Fuel Cell with and without Micro-Porous Layers

**Nguyen Ha Hiep**

Institute of Vehicle and Energy Engineering, Le Quy Don Technical University, Vietnam  
hahiepshippower@lqdtu.edu.vn

**Vu Duong**

School of Engineering and Technology, Duy Tan University, Vietnam  
duongvuaustralia@gmail.com (corresponding author)

Received: 2 February 2024 | Revised: 13 February 2024 | Accepted: 21 February 2024

Licensed under a CC-BY 4.0 license | Copyright (c) by the authors | DOI: <https://doi.org/10.48084/etasr.6996>

## ABSTRACT

This work presents the results of manufacturing a single Proton Exchange Membrane Fuel Cell (PEMFC) with Micro-Porous Layers (MPLs) and an active area of 25 cm<sup>2</sup>, and the experimental study required to build its polarization curve. Based on the physical model data, a numerical model of this PEMFC is created in the ANSYS PEM Fuel Cell module. Numerical simulations were performed with boundary conditions consistent with the experimental conditions on the test station. The calculation and experimental result comparison of the polarization curves for voltages ranging from 0.29 V to 0.94 V proved that the utilized numerical model is highly reliable. The simulation of PEMFC without MPLs was conducted according to such stable input parameters and boundary conditions. The results show that the PEMFC performance decreases significantly due to the flooding phenomenon inside PEMFC without MPLs compared to PEMFC with MPLs. Such phenomena are challenging to observe experimentally. Numerical modeling can be further used to optimize the fuel cell components.

*Keywords-fuel cell; micro-porous layer; current; flooding phenomenon; water content*

## I. INTRODUCTION

On December 13, 2023, the COP28 adopted a climate agreement calling for the world to move away from fossil fuels [1]. Alternative energy sources, such as hydrogen, and replacing burning fossil fuels energy conversion methods with electrochemical processes implemented in Fuel Cells (FCs), are encouraged to be utilized. Currently, there are several FC types: Proton Exchange Membrane (PEM), phosphoric acid, solid oxide, alkaline, and molten carbonate [2]. PEMFCs are more popular because they provide higher efficiency and energy density with low weight, volume, and noise and have a more straightforward structure [3]. PEMFCs can be used as a power source for FC electric vehicles and can be combined with batteries in hybrid electric vehicles [3]. In several studies, researchers have used FCs in power systems for vehicles [4-11], and physicochemical phenomena in FC and the influence of the components of FCs on their properties have been investigated [12-16]. Research on perfecting FCs and FC propulsion systems is increasingly vibrant and developing.

Through a PEMFC, the electric energy is derived from hydrogen and oxygen by electrochemical processes. The reagents are transferred to the reaction site in a PEMFC via supply channels. The hydrogen/oxygen reactions producing the oxidation of hydrogen and the reduction of oxygen are promoted in the Catalytic Layers (CLs). For a profitable PEMFC process, delivering a consistent allocation of the reagents in the electrode region and shunting to the collector of all catalyst particles is required to reduce ohmic losses. This procedure is continued by the Gas Diffusion Layer (GDL), which is placed suitably from the bipolar plate to the CL. An extra Micro-Porous Layer (MPL) can be adhered to the inner surface of a GDL, contacting with the CL to enhance the performance of GDL. The contacting resistance between the GDL and the CL can be decreased due to the MPL leads [14]. For PEMFC development, properties such as CLs, PEM, GDLs, MPLs, the number and configuration of channels on flow plates, operating conditions, etc. are the target of researchers to highlight their role in influencing PEMFC performance and internal phenomena.

This work aims to investigate the influence of the MPLs on PEMFC performance and the flooding phenomenon in PEMFCs. To do this, a PEMFC prototype was built using commercial materials and tests were conducted to measure its performance. The creation and calibration of this prototype model to obtain a polarization curve close to the experimental polarization curve and evaluate the model's reliability were conducted with the ANSYS PEM Fuel Cell Module (17.2 version, including upgrades). Then, the ANSYS model was numerically simulated and the flooding phenomenon inside the PEMFC was studied for both cases, with and without MPLs.

II. FABRICATING AND TESTING A FUEL CELL

A single PEMFC with MPL and an activated area of 25 cm<sup>2</sup> was developed using PEM (Nafion 212), GDLs + MPL (Sigracet 35BC), PTFE loading of 5 wt% and 25 wt% of GDL and MPL, respectively, 0.8 porosity [17, 18], CLs with 40 wt% Pt/C, and 40 wt% Nafion, and CL binder (Solution D520 5 wt%). The Membrane Electrode Assembly (MEA) was fabricated by hot pressing two electrodes onto both membrane sides at a temperature of 403 K and a pressure of 1.96 MPa for 180 s. The thickness of the MEA was 662 μm after hot pressing. The MEA was installed between two graphite bipolar plates (Graphite HK3), and 0.1 mm thick PTFE gaskets were placed between the contact surfaces. The graphite bipolar plates have serpentine grooves 1 mm wide and 1 mm deep. The MEA and graphite bipolar plate assembly was installed between the collector plates and then secured to the two housing plates with eight bolts (Figure 1). The PEMFC prototype was installed to the test bench, as shown in Figure 2. The mass flow controllers regulate the oxygen and hydrogen gas from the cylinders and pass through the hot water in humidifiers. Oxygen and hydrogen feed PEMFC has a constant relative humidity of 100% guaranteed by temperature regulation of the humidifier. A polarization curve of the PEMFC was evaluated in the Potentiostat.

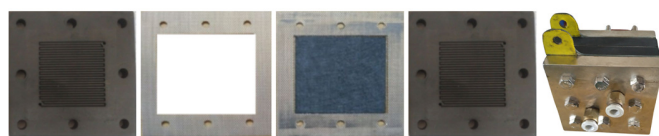


Fig. 1. The components and single PEMFC prototype.

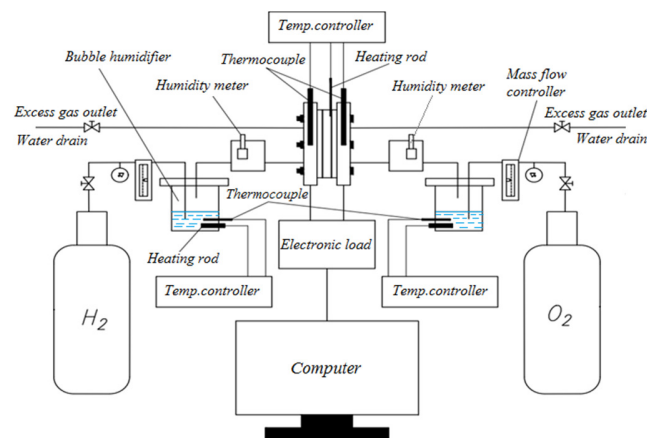


Fig. 2. The testing diagram of the PEMFC.

III. NUMERICAL STUDY

Assumptions and mathematical models for ANSYS PEMFC modeling are presented in [19]. Based on the physical model (Figure 1), a numerical model of PEMFC was created in the ANSYS. The geometric and mesh models (Figure 3) was built from about 7.4·10<sup>6</sup> elements and underwent many adjustments to obtain the desired convergence based on the meshing techniques mentioned in [20-24]. The simulation settings for the unsteady coefficients are pressure of 0.7, momentum of 0.3, and species of 0.95. The other parameters are equal to 1. The SIMPLE algorithm relates pressure and velocity to reference pressure discretization. A second-order bottom-up scheme was applied to discretize the other physicochemical and electrochemical quantities inside PEMFC. Simulations were performed until the current densities on the electrodes differed by less than 10<sup>-5</sup> mA/cm<sup>2</sup>, and the other criteria converged with 0.001% error. Cathode current densities were calculated by adjusting voltages from 0.29 to 0.94 V.

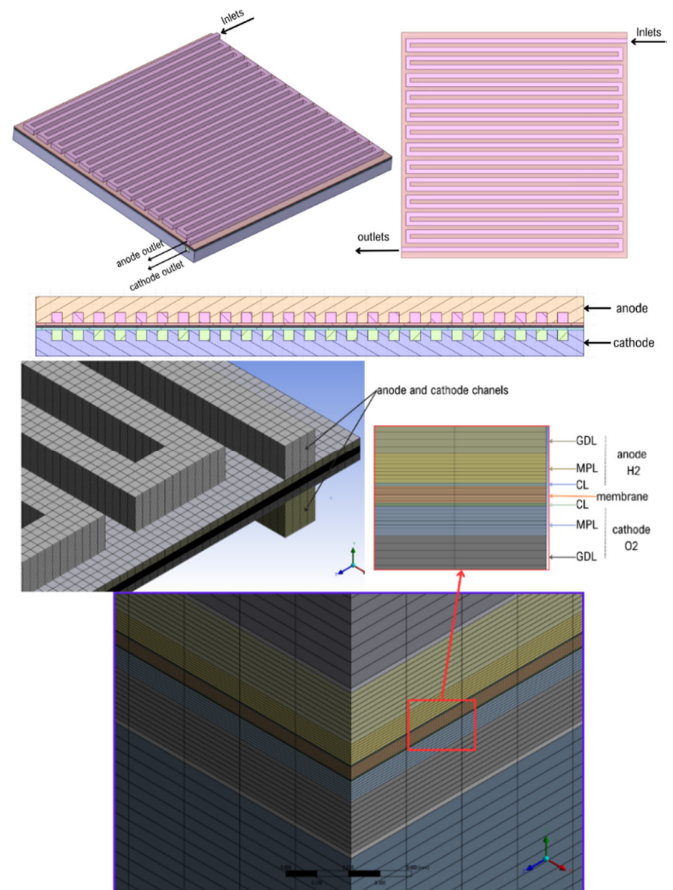


Fig. 3. The PEMFC geometric and meshing model

The input parameters for the simulation model are determined by (1)-(7).

The porosity of GDLs is determined by [25]:

$$\epsilon_{GDL} = 1 - (1 - \epsilon_0) \frac{\delta_0}{\delta} \tag{1}$$

The gas permeability of GDLs [ $\text{m}^2$ ] is evaluated by [26]:

$$K_{GDL} = \frac{\varepsilon_{GDL}}{8(\ln \varepsilon_{GDL})^2} \frac{(\varepsilon_{GDL} - \varepsilon_p)^{(\alpha+2)} d_f^2}{(1 - \varepsilon_p)^\alpha [(\alpha + 1)\varepsilon_{GDL} - \varepsilon_p]^2} \quad (2)$$

The MPL porosity and absolute permeability are also defined by (1) - (2), respectively. The CL volume fraction is calculated by [27]:

$$\varepsilon_{CL} = 1 - L_{Pt/C} - L_i \quad (3)$$

where  $L_{Pt/C}$  is determined by [15] (4) and  $f$  is the mass fraction of Pt, calculated by (5) [28]:

$$L_{Pt/C} = \frac{m_{pt}}{t_{CL}} \left( \frac{1}{\rho_{pt}} + \frac{1-f}{f} \frac{1}{\rho_c} \right) \times 10^4 \quad (4)$$

$$f = m_{pt} / (m_{pt} + m_c) \quad (5)$$

The ionomer content of Nafion in CLs is [29]:

$$W_{L_i} = V_N \rho_N \cdot 0.05 \quad (6)$$

$$L_i (\text{wt}\%) = 100 \cdot W_{L_i} / (W_{L_i} + W_{Pt/C})$$

The CL absolute permeability is [25]:

$$K_{CL} = \frac{d_p^2 \varepsilon_{CL}^3}{150(1 - \varepsilon_{CL})^2} \quad (7)$$

Table I presents the PEMFC component properties and the boundary conditions. The boundary conditions for the simulation model are consistent with the experimental conditions.

TABLE I. INPUT PARAMETERS AND BOUNDARY CONDITIONS

Parameter [Unit]	Symbol	Value	Reference
GDL (with MPL) thickness [m]	$\delta_0$	$325 \cdot 10^{-6}$	Fabricated
GDL porosity	$\varepsilon_0$	0.8	Fabricated
GDL thickness after hot pressing [m]	$\delta$	$275 \cdot 10^{-6}$	Fabricated
GDL fiber diameter [m]	$d_f$	$6.4 \cdot 10^{-6}$	[17]
Constants	$\varepsilon_p; \alpha$	0.037; 0.661	[26]
Platinum loading of CL [ $\text{mg}/\text{cm}^2$ ]	$m_{pt}$	0.4	Fabricated
Carbon loading of CL [ $\text{mg}/\text{cm}^2$ ]	$m_c$	0.6	Fabricated
CL initial thickness [m]	$t_{CL}$	$10^{-5}$	Fabricated
CL area [ $\text{cm}^2$ ]	$A_{CL}$	25	Fabricated
Pt/C weight of CL [g]	$W_{Pt/C}$	25	Fabricated
Pt and C densities [ $\text{kg}/\text{m}^3$ ]	$\rho_{pt}; \rho_c$	21450; 1800	[30]
Particle diameter of CL [m]	$d_p$	$2 \cdot 10^{-7}$	[31]
Nafion solution volume [ml]	$V_N$	363	Fabricated
Nafion solution density [ $\text{g}/\text{cm}^3$ ]	$\rho_N$	0.92	[29]
Relative humidity in electrodes [%]	-	100	Tested
Pressure in electrodes [Pa]	-	$0.2 \cdot 10^5$	Tested
Anode $\text{H}_2$ stoichiometry	-	1.5	Tested
Anode $\text{O}_2$ stoichiometry	-	2.0	Tested
Anode mass flow rate [g/s]	-	$7.8 \cdot 10^{-4}$	Tested
Cathode mass flow rate [g/s]	-	$6.4 \cdot 10^{-3}$	Tested
Temperature in electrodes [K]	-	348	Tested

#### IV. RESULTS AND DISCUSSION

The graphs of polarization curves, showing the voltage dependence on current density based on the experimental and simulation results are shown in Figure 4.

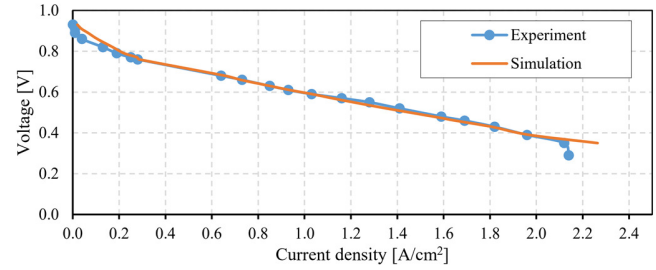
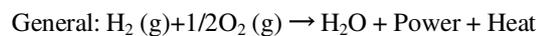
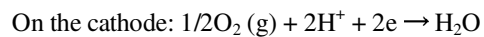
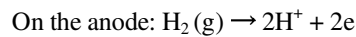


Fig. 4. Voltage-current density characteristics of PEMFC.

At lower current densities, the voltage decreases due to the activation energy required for the electrochemical reaction at the catalyst surface. The charge transfer coefficient and exchange current density mainly affect this region. After several adjustments based on the reference data in [15, 20, 22, 30], the studied model was appropriately adjusted. The voltage decreases linearly with current density at moderate current densities due to ohmic losses. The numerical and experimental result comparison shows that they are almost identical. Therefore, the input parameters have been calculated and selected correctly. At high current density, the rate of water formation at the cathode increases and causes flooding, and the formed water blocks the electrode holes, reducing the oxidant flow into the CL and causing the polarization curve to decrease sharply. The data in [19] determine the initial equilibrium water content at water saturation, adjusting the simulated polarization curve in this region to coincide with the experimental one.

Figure 4 shows a difference between the simulated and the experimental results at low current density, but the deviation is not more than 3%. At average current density, the simulation and experimental results coincide entirely. At the maximum current density, there is quite a difference between the results. However, they have high convergence overall within the research voltage range, from 0.29 to 0.94 V (as assumed in Section III), proving that the geometric model, input parameters, and boundary conditions are determined accurately and the built numerical model is highly reliable. In this study, we focus on the problem of PEMFC component flooding as a stated goal.

Figure 5 shows the water content of the main components, such as the cathode CL, membrane, and anode CL of the PEMFC with MPLs at a voltage of 0.39 V. Water is produced at the cathode as a result of the reaction in the PEMFC as follows:



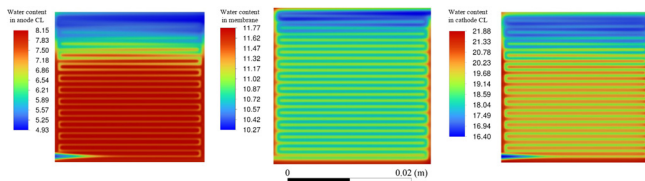


Fig. 5. Water contents on main PEMFC components

Water generated at the cathode will be discharged through grooves on the bipolar graphite plates of the cathode. Some of the water will penetrate the membrane, flow to the anode, and then exit through the groove on the bipolar graphite plates of the anode. If the water is not drained in time, it will cause flooding inside the PEMFC, which will hinder the reaction between oxygen and hydrogen and degrade the performance of the PEMFC. Good drainage is possible thanks to the groove structure of the graphite bipolar plates or the use of MPLs. Figure 6 illustrates water content in PEM for PEMFC with MPL and without MPL at 0.39 V. Without MPL, the amount of water stagnant in the membrane is more significant than when there is MPL. This shows that MPL improves water transport and increases the performance of PEMFCs (Figure 7).

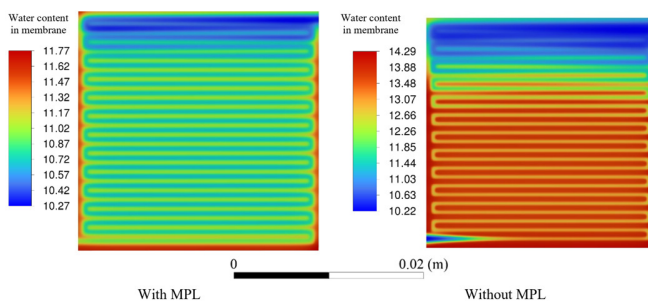


Fig. 6. Water contents in PEMs of the PEMFC with and without MPL.

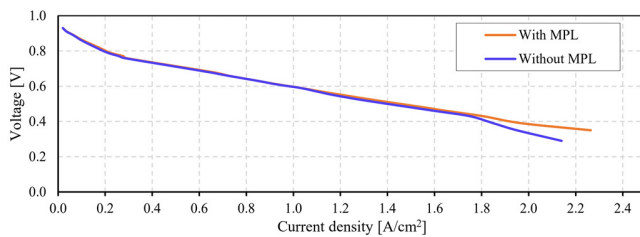


Fig. 7. Numerical polarization curves with and without MPL.

## V. CONCLUSIONS

In this study, a PEMFC prototype with MPLs was fabricated. The polarization curve of this PEMFC was developed during testing on the test station with calibrated equipment. The first novelty of this research was that a fuel cell prototype was built with good performance using suitable commercial components, considering parameters such as assembly force, pressing time, and pressing temperature. The second novelty is the provision of an accurate experimental data set that serves as a carefully calibrated input data set for calibrating similar models in practical fuel cell design and manufacturing.

The ANSYS software was applied to develop the numerical model of the PEMFC prototype. The numerical polarization curve obtained from the calibrated model agrees with the experimental data. The numerical model simulates the PEMFC without MPLs to evaluate the flooding phenomenon inside the PEMFC that is difficult to measure experimentally. The combination of experimental and numerical studies is critical in fuel cell development. Experiments are used to create samples and measure their characteristics. In contrast, numerical simulation reduces the number of samples that need to be manufactured, reduces the cost and time of complex experiments, and allows for observation and analysis of phenomena within the fuel cell, such as water transport and flooding. Observing these phenomena during experiments requires expensive measuring equipment, is difficult to implement, and is often impossible.

Another point of interest is that the published works of other authors [20-24] often consider GDL without MPLs when modeling with the ANSYS PEM Fuel Cell module. Our study highlighted this issue by adding MPLs. That is an inevitable matter in modern fuel cell technology.

A final novelty is that oxygen was used in this study as an oxidizing agent when modeling with the ANSYS PEM Fuel Cell module, which typically uses air as an oxidizer [20-24]. The use of oxygen requires certain representations of the input data.

In future studies, the numerical model can optimize the fuel cell properties, including Pt/C loading, Nafion loading in CLs, the porosity and permeability of GDL with or without MPLs, and the membrane thickness for developing and manufacturing high-performance fuel cells.

## ACKNOWLEDGMENT

This research is funded by Le Quy Don Technical University Research Fund under the grand number 2021.Q.04.

## REFERENCES

- [1] "COP28 Agreement Signals 'Beginning of the End' of the Fossil Fuel Era," *UNFCCC*. [https://unfccc.int/news/cop28-agreement-signals-beginning-of-the-end-of-the-fossil-fuel-era?gad\\_source=1&gclid=Cj0KCQiAxOauBhCaARIsAEBUSQRWASTPzA5aFB6zP-sEO\\_gwJE2Kg-3YAAaLVnNk4Hynw2ugUT4TyIYgaAlcgEALw\\_wcB](https://unfccc.int/news/cop28-agreement-signals-beginning-of-the-end-of-the-fossil-fuel-era?gad_source=1&gclid=Cj0KCQiAxOauBhCaARIsAEBUSQRWASTPzA5aFB6zP-sEO_gwJE2Kg-3YAAaLVnNk4Hynw2ugUT4TyIYgaAlcgEALw_wcB).
- [2] M. Marappan *et al.*, "Performance Studies of Proton Exchange Membrane Fuel Cells with Different Flow Field Designs – Review," *The Chemical Record*, vol. 21, no. 4, pp. 663–714, 2021, <https://doi.org/10.1002/tcr.202000138>.
- [3] C. Spiegel, *Designing and Building Fuel Cells*. New York, NY, USA: McGraw Hill, 2007.
- [4] A. Khadhraoui, T. Selmi, and A. Cherif, "Energy Management of a Hybrid Electric Vehicle," *Engineering, Technology & Applied Science Research*, vol. 12, no. 4, pp. 8916–8921, Aug. 2022, <https://doi.org/10.48084/etasr.5058>.
- [5] S. N. M., O. Tremblay, and L.-A. Dessaint, "A generic fuel cell model for the simulation of fuel cell vehicles," in *IEEE Vehicle Power and Propulsion Conference*, Dearborn, MI, USA, Sep. 2009, pp. 1722–1729, <https://doi.org/10.1109/VPPC.2009.5289692>.
- [6] S. N. Motapon, O. Tremblay, and L.-A. Dessaint, "Development of a generic fuel cell model: application to a fuel cell vehicle simulation," *International Journal of Power Electronics*, vol. 4, no. 6, pp. 505–522, Jan. 2012, <https://doi.org/10.1504/IJPELEC.2012.052427>.

- [7] C. Spiegel, *PEM Fuel Cell Modeling and Simulation Using MATLAB*. London, UK: Academic Press, 2008.
- [8] S. Javadpoor and D. Nazarpour, "Modeling a PV-FC-Hydrogen Hybrid Power Generation System," *Engineering, Technology & Applied Science Research*, vol. 7, no. 2, pp. 1455–1459, Apr. 2017, <https://doi.org/10.48084/etasr.760>.
- [9] J. Chakravorty, J. Saraswat, and V. Bhatia, "Modeling a Distributed Power Flow Controller with a PEM Fuel Cell for Power Quality Improvement," *Engineering, Technology & Applied Science Research*, vol. 8, no. 1, pp. 2585–2589, Feb. 2018, <https://doi.org/10.48084/etasr.1807>.
- [10] S. Barhate, R. Mudhalwadkar, and S. Madhe, "Fault Detection Methods Suitable for Automotive Applications in Proton Exchange Fuel Cells," *Engineering, Technology & Applied Science Research*, vol. 12, no. 6, pp. 9607–9613, Dec. 2022, <https://doi.org/10.48084/etasr.5262>.
- [11] M. A. Biberici and M. B. Celik, "Dynamic Modeling and Simulation of a PEM Fuel Cell (PEMFC) during an Automotive Vehicle's Driving Cycle," *Engineering, Technology & Applied Science Research*, vol. 10, no. 3, pp. 5796–5802, Jun. 2020, <https://doi.org/10.48084/etasr.3352>.
- [12] H. Bouzidi, L. Otmani, R. Doufnoune, L. Zerroual, and D. Benachour, "Influence of Membrane Type on Some Electrical Properties of a Single Microbial Fuel Cell," *Engineering, Technology & Applied Science Research*, vol. 12, no. 3, pp. 8492–8499, Jun. 2022, <https://doi.org/10.48084/etasr.4813>.
- [13] G. Sasikumar, J. W. Ihm, and H. Ryu, "Dependence of optimum Nafion content in catalyst layer on platinum loading," *Journal of Power Sources*, vol. 132, no. 1, pp. 11–17, May 2004, <https://doi.org/10.1016/j.jpowsour.2003.12.060>.
- [14] C.-J. Tseng and S.-K. Lo, "Effects of microstructure characteristics of gas diffusion layer and microporous layer on the performance of PEMFC," *Energy Conversion and Management*, vol. 51, no. 4, pp. 677–684, Apr. 2010, <https://doi.org/10.1016/j.enconman.2009.11.011>.
- [15] N. Khajeh-Hosseini-Dalasm, M. J. Kermani, D. G. Moghaddam, and J. M. Stockie, "A parametric study of cathode catalyst layer structural parameters on the performance of a PEM fuel cell," *International Journal of Hydrogen Energy*, vol. 35, no. 6, pp. 2417–2427, Mar. 2010, <https://doi.org/10.1016/j.ijhydene.2009.12.111>.
- [16] N. H. Hiep, N. Q. Quan, G. H. Thai, and P. T. San, "Numerical Modeling and Experimental Validation of a Hydrogen/Oxygen Fuel Cell for Underwater Vehicle Applications," SAE International, Warrendale, PA, USA, SAE Technical Paper 2023-01–5053, Aug. 2023, <https://doi.org/10.4271/2023-01-5053>.
- [17] A. Pfrang, S. Didas, and G. Tsotridis, "X-ray computed tomography of gas diffusion layers of PEM fuel cells: Segmentation of the microporous layer," *Journal of Power Sources*, vol. 235, pp. 81–86, Aug. 2013, <https://doi.org/10.1016/j.jpowsour.2013.01.179>.
- [18] F. Aldakheel *et al.*, "Gas permeability, wettability and morphology of gas diffusion layers before and after performing a realistic ex-situ compression test," *Renewable Energy*, vol. 151, pp. 1082–1091, May 2020, <https://doi.org/10.1016/j.renene.2019.11.109>.
- [19] ANSYS FLUENT Theory Guide 17.2. Canonsburg, PA, USA: ANSYS, 2022.
- [20] M. Arif, S. C. P. Cheung, and J. Andrews, "A systematic approach for matching simulated and experimental polarization curves for a PEM fuel cell," *International Journal of Hydrogen Energy*, vol. 45, no. 3, pp. 2206–2223, Jan. 2020, <https://doi.org/10.1016/j.ijhydene.2019.11.057>.
- [21] I. Nitta, S. Karvonen, O. Himanen, and M. Mikkola, "Modelling the Effect of Inhomogeneous Compression of GDL on Local Transport Phenomena in a PEM Fuel Cell," *Fuel Cells*, vol. 8, no. 6, pp. 410–421, 2008, <https://doi.org/10.1002/fuce.200700058>.
- [22] M. Arif, S. C. P. Cheung, and J. Andrews, "Numerical investigation of effects of different flow channel configurations on the 100 cm<sup>2</sup> PEM fuel cell performance under different operating conditions," *Catalysis Today*, vol. 397–399, pp. 449–462, Aug. 2022, <https://doi.org/10.1016/j.cattod.2021.07.016>.
- [23] M. Arif, S. C. P. Cheung, and J. Andrews, "Influence of Hydrophobicity and Porosity of the Gas Diffusion Layer on Mass Transport Losses in PEM Fuel Cells: A Simulation Study Supported by Experiments," *Energy & Fuels*, vol. 34, no. 10, pp. 13010–13022, Oct. 2020, <https://doi.org/10.1021/acs.energyfuels.0c02596>.
- [24] W. Xiaofei, Q. Yang, Z. Zhigang, and X. Liusheng, "Investigation of Ship Vibration Effects on the Gas Distribution and Output Voltage of a Proton Exchange Membrane Fuel Cell," *ACS Omega*, vol. 7, no. 24, pp. 20569–20583, Jun. 2022, <https://doi.org/10.1021/acsomega.2c00273>.
- [25] J. Zhao, S. Shahgaldi, I. Alaefour, Q. Xu, and X. Li, "Gas permeability of catalyzed electrodes in polymer electrolyte membrane fuel cells," *Applied Energy*, vol. 209, pp. 203–210, Jan. 2018, <https://doi.org/10.1016/j.apenergy.2017.10.087>.
- [26] J. T. Gostick, M. W. Fowler, M. D. Pritzker, M. A. Ioannidis, and L. M. Behra, "In-plane and through-plane gas permeability of carbon fiber electrode backing layers," *Journal of Power Sources*, vol. 162, no. 1, pp. 228–238, Nov. 2006, <https://doi.org/10.1016/j.jpowsour.2006.06.096>.
- [27] A. A. Shah, G.-S. Kim, P. C. Sui, and D. Harvey, "Transient non-isothermal model of a polymer electrolyte fuel cell," *Journal of Power Sources*, vol. 163, no. 2, pp. 793–806, Jan. 2007, <https://doi.org/10.1016/j.jpowsour.2006.09.022>.
- [28] M. Secanell, K. Karan, A. Suleman, and N. Djilali, "Multi-variable optimization of PEMFC cathodes using an agglomerate model," *Electrochimica Acta*, vol. 52, no. 22, pp. 6318–6337, Jun. 2007, <https://doi.org/10.1016/j.electacta.2007.04.028>.
- [29] G. Adilbish and Y.-T. Yu, "Effect of the Nafion content in the MPL on the catalytic activity of the Pt/C-Nafion electrode prepared by pulsed electrophoresis deposition," *International Journal of Hydrogen Energy*, vol. 42, no. 2, pp. 1181–1188, Jan. 2017, <https://doi.org/10.1016/j.ijhydene.2016.09.143>.
- [30] S. Li, J. Yuan, M. Andersson, G. Xie, and B. Sundén, "Influence of anisotropic gas diffusion layers on transport phenomena in a proton exchange membrane fuel cell," *International Journal of Energy Research*, vol. 41, no. 14, pp. 2034–2050, 2017, <https://doi.org/10.1002/er.3763>.
- [31] S. Li, J. Yuan, G. Xie, and B. Sundén, "Effects of agglomerate model parameters on transport characterization and performance of PEM fuel cells," *International Journal of Hydrogen Energy*, vol. 43, no. 17, pp. 8451–8463, Apr. 2018, <https://doi.org/10.1016/j.ijhydene.2018.03.106>.